A Combined Experimental and Computational Exploration of Heteroleptic cisPd2L2L’2 Coordination Cages through Geometric Complementarity

Chemistry–A European Journal
Research Article
doi.org/10.1002/chem.202403336
Chemistry Europe
European Chemical Societies Publishing
www.chemeurj.org

Hot Paper

A Combined Experimental and Computational Exploration of Heteroleptic *cis*-$Pd_2L_2L'_2$ Coordination Cages through Geometric Complementarity

Andrew Tarzia,*[a] Wentao Shan,[b] Victor Posligua,[b] Cameron J. T. Cox,[c] Louise Male,[c] Benjamin D. Egleston,[b] Rebecca L. Greenaway,[b] Kim E. Jelfs,[b] and James E. M. Lewis*[c]

Heteroleptic (mixed-ligand) coordination cages are of interest as host systems with more structurally and functionally complex cavities than homoleptic architectures. The design of heteroleptic cages, however, is far from trivial. In this work, we experimentally probed the self-assembly of Pd(II) ions with binary ligand combinations in a combinatorial fashion to search for new *cis*-$Pd_2L_2L'_2$ heteroleptic cages. A hierarchy of computational analyses was then applied to these systems with the aim of elucidating key factors for rationalising self-assembly outcomes. Simple and inexpensive geometric analyses were shown to be effective in identifying complementary ligand pairs. Preliminary results demonstrated the viability of relatively rapid semi-empirical calculations for predicting the topology of thermodynamically favoured assemblies with rigid ligands, whilst more flexible systems proved challenging. Stemming from this, key challenges were identified for future work developing effective computational forecasting tools for self-assembled metallo-supramolecular systems.

Metal-organic, or coordination, cages (MOCs)[1] are generally prepared from single metal ions/nodes and single, high-symmetry ligands. This simple recipe has yielded cages of varying size, nuclearity and geometry, and their use in catalysis,[2] stabilisation of reactive species,[3] molecular separations[4] and encapsulation of anions[5] and pollutants,[6] amongst others. More structurally sophisticated, reduced symmetry architectures,[7] however, offer the potential for precision engineering of MOC hosts.[8] As such, there has been increasing interest in targeting low-symmetry MOCs.

M_2L_4-type cages,[9] first reported by McMorran and Steel,[10] have become one of the most popular classes of MOCs. Strategies to prepare lower symmetry congeners of these include assembly from reduced symmetry ligands,[11] and forming heteronuclear[12] and heteroleptic[13] architectures.

Heteroleptic MOCs form when mixtures of ligands (**L** and **L'**) preferentially self-assemble into defined mixed-ligand structures (integrative self-sorting) rather than their homoleptic species (narcissistic self-sorting) or a statistical mixture (Figure 1a). Heteroleptic cages are especially attractive due to the potential to incorporate multiple functional units using different ligand scaffolds.[14] Two main approaches towards heteroleptic M_2L_4 MOCs have been reported. *Coordination-sphere engineering* (also termed *side-chain directing*)[15] exploits interactions between ligands to promote integrative self-assembly, e.g. through steric repulsion,[16] hydrogen-bonding[17] or ancillary coordinating groups.[18] Clever and co-workers have pioneered *geometric complementarity* between ligands as an alternative strategy (Figure 1b). Two ligands, one with a convergent coordination mode (**L**), the other divergent (**L'**), if appropriately size-matched, can successfully assemble to give the desired

[a] Dr. A. Tarzia
Department of Applied Science and Technology, Politecnico di Torino, Corso Duca degli Abruzzi 24, 10129 Torino, Italy
E-mail: andrew.tarzia@polito.it
Homepage: https://andrewtarzia.github.io/
[b] W. Shan, Dr. V. Posligua, Dr. B. D. Egleston, Dr. R. L. Greenaway, Prof. Dr. K. E. Jelfs
Department of Chemistry, Imperial College London, Molecular Sciences Research Hub, White City Campus, Wood Lane, London W12 0BZ, UK
[c] C. J. T. Cox, Dr. L. Male, Dr. J. E. M. Lewis
School of Chemistry, University of Birmingham, Edgbaston, Birmingham B15 2TT, UK
E-mail: j.e.m.lewis@bham.ac.uk
Homepage: https://lewisgroup.org.uk/

Supporting information for this article is available on the WWW under https://doi.org/10.1002/chem.202403336

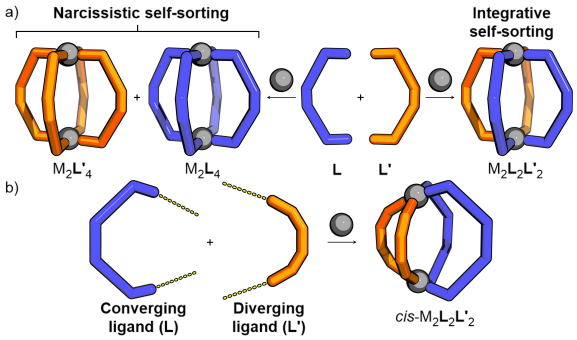

Figure 1. a) Ditopic ligands **L** (blue) and **L'** (orange) can self-assemble with narcissistic self-sorting (left), forming their respective homoleptic species, or integrative sorting (right) to form heteroleptic structures. b) One approach to promote integrative self-sorting is to design ligands with converging (blue) and diverging (orange) coordination vectors that exhibit geometric complementary to each other.

heteroleptic cage ($Pd_2\mathbf{L}_2\mathbf{L'}_2$).[19] Further developments to this strategy have yielded higher nuclearity systems with binary combinations of ligands,[20] and systems incorporating three[21] or even four[22] different ligand frameworks.

Although the geometric approach is highly intuitive, designing complementary ligand pairs remains a significant challenge. Recently, chemists have begun exploring high-throughput computational approaches to aid in the design of MOC systems[23] (and rationalise properties).[24] Computational forecasting would reduce traditional trial-and-error strategies that can be especially costly and time-consuming for structurally sophisticated assemblies. For example, by mapping ligands onto a wide range of defined topological templates ($n = 3$–30) and comparing their relative computed energies, Reek and co-workers were able to accurately predict the nuclearity of large Pd_nL_{2n} polyhedra.[25] We have previously demonstrated computationally-informed design in targeting isomers of Pd_2L_4 MOCs assembled from unsymmetrical ditopic ligands using low-cost semi-empirical methods.[26] We have now tried to expand this approach to heteroleptic cage systems.

In this work, we attempt to establish a protocol using rapidly computed data to allow efficient forecasting of integrative self-assembly of ligands to form heteroleptic MOCs. To achieve this goal, the self-assembly of binary combinations of ditopic ligands with Pd(II) ions was examined experimentally. From the twelve possible ligand combinations, two pairs were observed to cleanly form heteroleptic *cis*-$Pd_2\mathbf{L}_2\mathbf{L'}_2$ cages. A hierarchy of calculations of varying computational expense were then used to rationalise the self-assembly outcomes. While ligand-based approaches proved effective in mirroring experimental data, cage-based analyses uncovered limitations in the modelling process of great importance for the computationally-aided design of MOCs.

Results & Discussion

Ligand Selection and Synthesis

To dissect key factors in the design of heteroleptic metal-organic assemblies, both positive (integrative self-assembly) and negative (narcissistic/non-specific self-assembly) results would be of use. Unfortunately for our purposes, negative data, i.e. statistical self-assembly or otherwise undesirable self-sorting outcomes, are infrequently published. Due to this paucity of data, we sought to generate our own to fill this gap. Specifically targeting *cis*-$Pd_2\mathbf{L}_2\mathbf{L'}_2$ heteroleptic cages in this work, three diverging (**1**) and four converging ligands (**2**) were chosen that possessed core aromatic units of different sizes and angles between the connectivity points of the donor units, and different accessible distances between the coordinating atoms of the donors (Figure 2 and see conformer discussion below).

The three diverging ligands, $\mathbf{1}^{DBF}$,[27] $\mathbf{1}^{Ph}$,[28] and $\mathbf{1}^{Th}$[29] have been previously reported. Four novel converging ligands with isoquinoline coordinating units, namely $\mathbf{2}^{DBF}$, $\mathbf{2}^{Py}$, $\mathbf{2}^{Ph}$ and $\mathbf{2}^{Th}$, were prepared using standard synthetic procedures (ESI section S2) and their identities confirmed by NMR and high-resolution electrospray ionisation mass spectrometry (HR-ESI-MS).

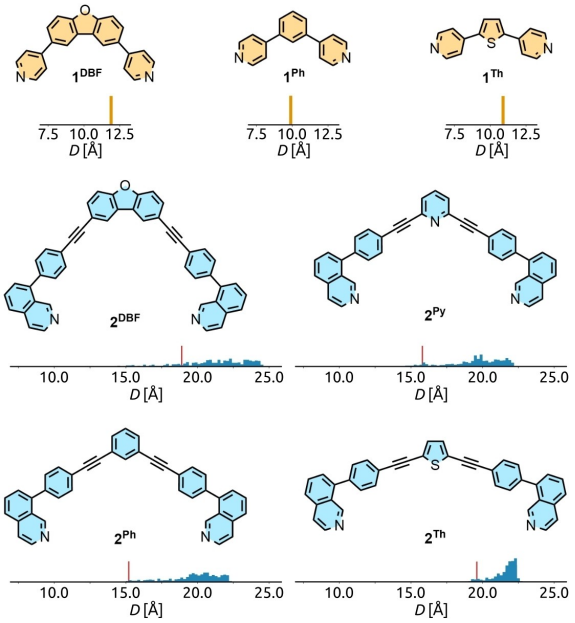

Figure 2. Structures of diverging ligands **1** and converging ligands **2**. Each structure includes the distribution of N–N distances over conformers generated (see below) within 5 kJ mol^{-1} of the lowest energy conformer. For ligands **2**, conformers closest to the "as-drawn" planar structure indicated by red lines.

Homoleptic Self-Assembly

Initially, an examination of homoleptic self-assembly was undertaken. Diverging ligands $\mathbf{1}^{DBF}$, $\mathbf{1}^{Ph}$ and $\mathbf{1}^{Th}$ have been previously reported to self-assemble with Pd(II) ions into a Pd_6L_{12} cube,[27] $Pd_{12}L_{24}$ cuboctahedron[28] and $Pd_{30}L_{60}$ icosidodecahedron[29] (with a $Pd_{24}L_{48}$ rhombicuboctahedron[30] forming as a kinetically-trapped species), respectively.

The novel, converging ligands, **2**, were each combined with $[Pd(CH_3CN)_4](BF_4)_2$ in a 2:1 ratio in d_6-DMSO (0.04 M ligand concentration). After equilibrating, the identities of the products formed were probed by NMR and MS.

For $\mathbf{2}^{Th}$, formation of a quadruply-stranded $[Pd_2(\mathbf{2}^{Th})_4]^{4+}$ cage was concluded based on NMR (e.g. downfield shifts of the *ortho*-pyridyl protons, Figure S53), diffusion-orientated spectroscopy (DOSY; $R_S \approx 12$ Å) and ESI-MS data (Figures S59–S62). For $\mathbf{2}^{DBF}$, following initial dissolution, a precipitate was observed to form. After filtration, ^{1}H NMR analysis of the solution revealed the internally-directed *ortho*-isoquinoline proton to be shifted significantly upfield relative to the free ligand (Figure S93), indicative of π-stacking. The NMR data, in combination with ESI-MS, were congruent with formation of a helical Pd_2L_4 assembly.[31]

A broad and messy ^{1}H NMR spectrum was observed at room temperature from the self-assembly mixture with $\mathbf{2}^{Ph}$, with DOSY suggesting formation of at least two species ($R_S \approx 11$ and 13 Å). At 80 °C the ^{1}H NMR spectrum sharpened dramatically to

reveal a set of predominant signals (Figure S79). Upfield shifts of some signals relative to the ligand (Figure S80) were consistent with a helical Pd_2L_4 architecture. This was supported by ESI-MS, from which additional signals for a Pd_3L_6 assembly could also be seen (Figures S85–S92). Thus, a mixture of species, including a Pd_2L_4 cage and a Pd_3L_6 assembly, appeared to have formed.

In the case of $\mathbf{2}^{Py}$, isotopic patterns consistent with the formulation $[Pd_3(\mathbf{2}^{Py})_6]^{6+}$ were exclusively observed by ESI-MS (Figures S71–S76). The ^{1}H NMR spectrum had overlapping peaks, although DOSY suggested formation of a main species with $R_S = 13.5$ Å. Upon heating the sample to 80 °C, a sharpening and shift in the resonances of some signals was observed, leading to less overlap (Figure S65), with 15 proton environments becoming apparent. It was concluded that the major assembly was likely a trinuclear architecture with the two ends of the ligands occupying distinct environments.[32] Interestingly, when the SCXRD structure was solved from weakly diffracting crystals, the solid-state structure was shown to be a Pd_2L_4 helicate[31] (Figure 3).

Heteroleptic Self-Assembly

A combinatorial approach was taken to experimentally examine self-assembly of binary mixtures of ligands with Pd(II). The 12 possible combinations of a 1:1:1 mixture of **1**, **2** and $[Pd(CH_3CN)_4](BF_4)_2$ were sonicated in d_6-DMSO until a homogenous solution was obtained, and subsequently heated at 50 °C until no further spectroscopic changes were observed by ^{1}H NMR.

All combinations with $\mathbf{1}^{Ph}$ and $\mathbf{1}^{Th}$ only showed formation of homoleptic assemblies (ESI section S3). The mixture of $\mathbf{1}^{DBF}$ and $\mathbf{2}^{Th}$ gave three distinct species (Figures S151–S153) consisting of the two homoleptic cages and a third assembly identified by ESI-MS (Figure S155) as the heteroleptic $[Pd_2(\mathbf{1}^{DBF})_2(\mathbf{2}^{Th})_2]^{4+}$ architecture. Prolonged heating (3 d at 60 °C) led to almost complete conversion to the homoleptic systems, with further elevated temperatures (70 °C) resulting in sample degradation. Thus $[Pd_2(\mathbf{1}^{DBF})_2(\mathbf{2}^{Th})_2]^{4+}$ appeared to form as a kinetic product, although it could not be ruled out that the difference in energy with the homoleptic systems was very small.

The combination of $\mathbf{1}^{DBF}$ with $\mathbf{2}^{Py}/\mathbf{2}^{Ph}$ gave NMR spectra indicating clean formation of single species distinct from the homoleptic assemblies (Figure 4a and b, respectively), with a 1:1 ratio of the two ligands. DOSY showed all ligand signals diffused at the same rate, indicative of being part of a single assembly (Figures S104 and S129). Through-space interactions between the *ortho*-pyridyl/isoquinolyl protons of ligands **1** and **2** were observed by nuclear Overhauser effect spectroscopy (NOESY; Figure 4c). Finally, isotopic patterns observed by ESI-MS were consistent with the formulation $\{[Pd_2(\mathbf{1}^{DBF})_2(\mathbf{2}^{Py}/\mathbf{2}^{Ph})_2](X^-)_n\}^{(4-n)+}$ (Figures S105 and S130). All told, the spectroscopic data led to the conclusion that successful integrative self-assembly had yielded $Pd_2\mathbf{L}_2\mathbf{L'}_2$ heteroleptic assemblies. Disappointingly, all attempts to grow X-ray quality single crystals of the cages were unsuccessful. DFT-optimised structures (Figure 4e) of both *cis*-$Pd_2\mathbf{L}_2\mathbf{L'}_2$ cages revealed no extraordinary distortion of the ligand frameworks or Pd(II) coordination environment.

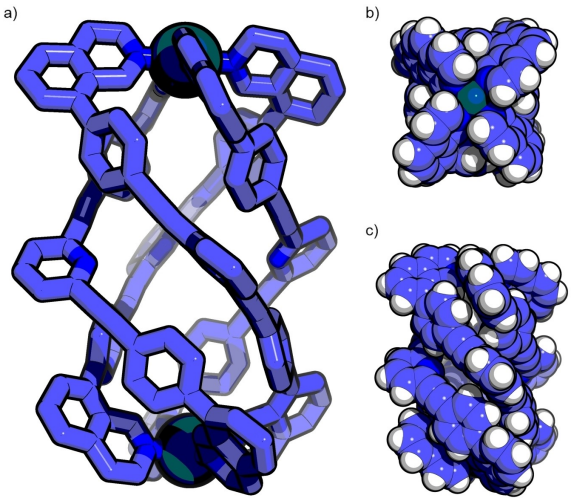

Figure 3. SCXRD structure of the Λ enantiomer of $[Pd_2(\mathbf{2}^{Py})_4]^{4+}$ a) from the side, with hydrogen atoms omitted for clarity, and space-fill models shown b) down the Pd···Pd axis, and c) from the side.

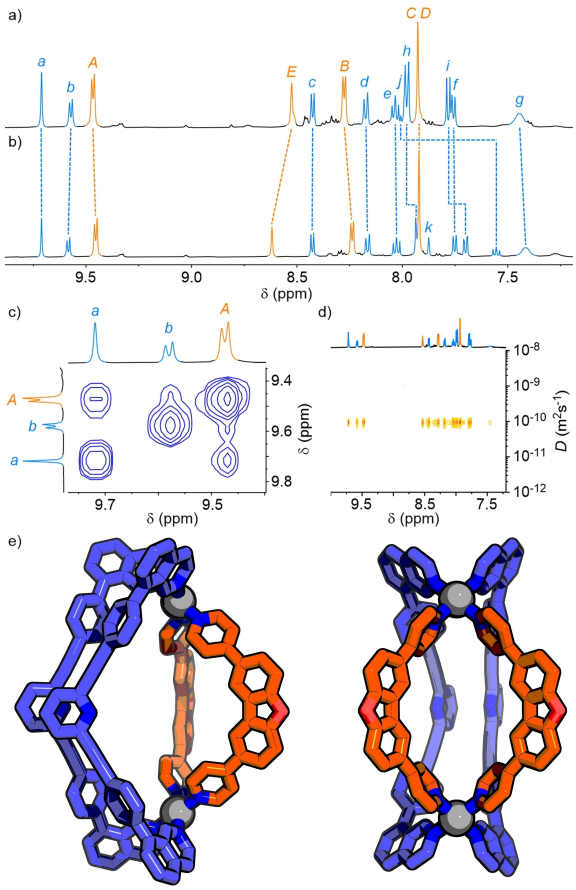

Figure 4. ^{1}H NMR spectra (500 MHz, d_6-DMSO, 298 K) of a) $[Pd_2(\mathbf{1}^{DBF})_2(\mathbf{2}^{Py})_2](BF_4)_4$ and b) $[Pd_2(\mathbf{1}^{DBF})_2(\mathbf{2}^{Ph})_2](BF_4)_4$; c) partial NOESY of $[Pd_2(\mathbf{1}^{DBF})_2(\mathbf{2}^{Py})_2](BF_4)_4$ showing interactions between ligands $\mathbf{1}^{DBF}$ and $\mathbf{2}^{Py}$, and d) DOSY of $[Pd_2(\mathbf{1}^{DBF})_2(\mathbf{2}^{Py})_2](BF_4)_4$. e) DFT-optimised structure (PBE0/Def2-SVP/D3BJ/PCM(DMSO)) of *cis*-$[Pd_2(\mathbf{1}^{DBF})_2(\mathbf{2}^{Py})_2]^{4+}$.

Confirmation that the heteroleptic cages formed were thermodynamic products was sought through a cage-to-cage transformation experiment. d_6-DMSO solutions of $[Pd_6\mathbf{1}^{DBF}{}_{12}](BF_4)_{12}$ and $[Pd_2\mathbf{2}^{Py}{}_4](BF_4)_4$ were combined and stood at elevated temperatures. Although extremely slow (>3 weeks to reach 50% conversion at 50 °C), continued conversion to the heteroleptic $[Pd_2\mathbf{1}^{DBF}{}_2\mathbf{2}^{Py}{}_2](BF_4)_4$ species was observed (Figure S136).

Having experimentally investigated the integrative self-assembly of pairs of converging and diverging ligands, we turned to computational analysis of these structures in the search for underlying guidelines that might help in the future design of heteroleptic assemblies.

Geometric Analysis of Ligand Combinations

As a simple probe of the "goodness-of-fit" between pairs of ligands, a geometric model was initially considered. The coordination of **1** and **2** *trans* to each other across Pd(II) ions was equated to a planar trapezoid (Figure 5). The lengths (D) of the two parallel sides relate to the distance between coordinating atoms for the diverging ligand **1** (D_d) and the converging ligand **2** (D_c). Assuming a Pd–N distance of 2.02 Å (mean distance from CSD; ESI section S4), the remaining two sides would each be equal to 4.04 Å. The angles between coordinating groups (Θ; Figure 5) for both the converging (Θ_c) and diverging ligands (Θ_d) thus make up the four internal angles of the trapezoid. With the D and Θ values known for one ligand, it is possible to calculate corresponding idealised values for a perfectly matched partner ligand.

To account for conformational flexibility, a library of 500 conformers was generated for each ligand, using the ETKDG (version 3, srETKDGv3) algorithm[33] within the open-source cheminformatics software RDKit.[34] Geometry optimisation for each conformer was then performed using the universal force-field (UFF).[35] After removing unsuitable conformations (see ESI section S4 for details),[36] filtered libraries of 4–34 conformers per ligand were obtained (Table S1).

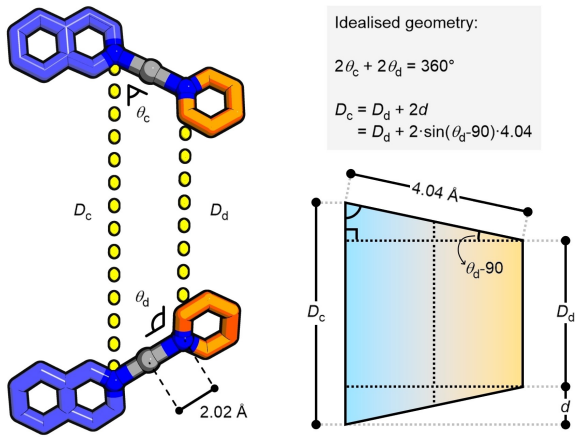

Figure 5. Cartoon representation of the coordination angles within an idealised heteroleptic *cis*-$Pd_2\mathbf{L}_2\mathbf{L'}_2$ assembly.

From these libraries, data for each of the conformers (Θ and D values) was extracted. For the more rigid, diverging ligands **1**, geometry values of idealised partner ligands were calculated for each of the conformers. These were then compared in a combinatorial fashion against the values for the computed conformers of ligands **2**, allowing an examination of their deviation from the ideal with respect to both the N···N distance and angle of the coordinating groups. This yielded 12 sets of angle deviation (a) and length deviation (l) values (Figure 6) for the possible combinations of **1** and **2** (each with 108–544 conformer pairs). With complementary pairs of ligand conformers ideally having a and l values near 1, plotting this data would allow for simple visual searches for pairs of ligands with multiple complementary conformers (Figure 6a–c).

It was seen that the two systems that successfully underwent integrative self-assembly (i.e. $\mathbf{1}^{DBF}$ and $\mathbf{2}^{Py}$/$\mathbf{2}^{Ph}$) clustered close to the intercept, representative of near-ideal geometries (Figure 6a). Conversely, those that exhibited narcissistic self-assembly (e.g. Figure 6b and Figure S167) generally had conformer distributions away from the ideal. The combination of $\mathbf{1}^{DBF}$ and $\mathbf{2}^{DBF}$ was a notable exception to this (Figure 6c).

It was then attempted to condense this data into more readily processable information. From the density maps, the distance from $a = l = 1$ for each pair of conformers could be readily calculated, providing a single value, termed the deviation factor, g, composed of both length (l) and angle (a) deviation components. In this manner, a set of g values was derived for each combination of **1** and **2**, from which an average value (g_{avg}) was calculated (Figure 6d). Pleasingly, $\mathbf{1}^{DBF}$ paired with $\mathbf{2}^{Py}$ and $\mathbf{2}^{Ph}$ gave some of the lowest g_{avg} values (0.35 and 0.34, respectively). Whilst most other ligand combinations exhibited higher g_{avg} values (≥0.7), the combination of $\mathbf{1}^{DBF}$ and $\mathbf{2}^{Th}$, which had formed the heteroleptic species to some extent, also possessed a low g_{avg} (0.33).

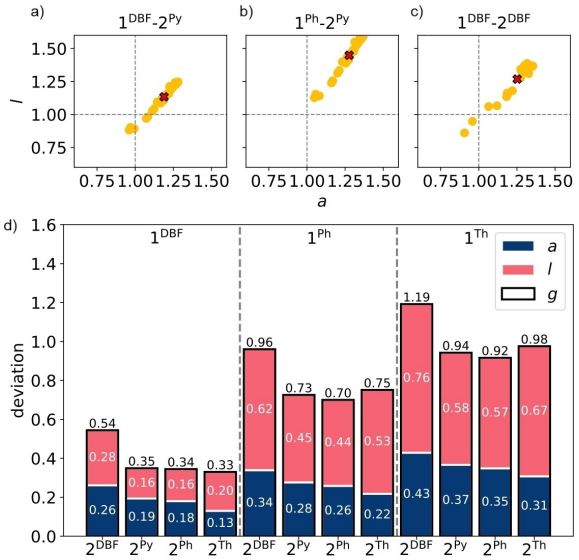

Figure 6. Plots of angle (a) and length (l) deviations for conformer libraries of a) $\mathbf{1}^{DBF}$ and $\mathbf{2}^{Py}$, b) $\mathbf{1}^{Ph}$ and $\mathbf{2}^{Py}$, and c) $\mathbf{1}^{DBF}$ and $\mathbf{2}^{DBF}$. Red crosses denote average a and l values. d) Charts of average deviation values for all ligand combinations.

To further explore the viability of *g* values for identifying promising ligand pairs, analyses of several *cis*-$Pd_2\mathbf{L}_2\mathbf{L'}_2$ systems from the literature were undertaken. Pleasingly, these previously reported systems were also generally shown to give low g_{avg} values (< 0.6) (ESI section S5). From this analysis g_{avg} tended towards smaller values in successful heteroleptic candidates. Given the simplicity of this metric, which does not consider chemical or physical features of the ligands, it is unsurprising, however, that a range of values (~0.3–0.6) were observed.

This computationally efficient screening procedure successfully highlighted promising candidates for heteroleptic cage formation. Crucially, a large proportion of ligand combinations that did not form heteroleptic assemblies (i.e. true negatives) were identifiable and could reasonably be excluded. This low-cost approach can be run on a common laptop based only on UFF geometry optimisations of the ligand conformers. Conformer generation is achieved in minutes, whilst geometric matchings between conformers takes seconds. As such, this screening tool is viable for high-throughput analysis of large ligand libraries. The code for running this analysis has been made freely available,[37] only requiring ligand SMILES strings as input.

It is noted that the idealised trapezoid geometry used in this model is not necessarily suited to alternative heteroleptic MOC architectures. Rather than provide a generic system for expansive exploration of chemical space, this approach was intended to be used for expediting the successful realisation of targeted metal-organic systems – in this instance, *cis*-$Pd_2\mathbf{L}_2\mathbf{L'}_2$ cages specifically. It is anticipated that the core concepts, however, could be adapted to provide similar, rapid geometric analysis for alternative system designs.

Computational Analysis of Assembly Energies

Ultimately, it would be desirable to develop a robust, high-throughput computational workflow for rapidly assessing the likelihood of integrative self-assembly using calculated energies of the MOCs. The rationale is that this approach should encapsulate more factors than simply geometric complementarity between ligands, providing a more sophisticated approach to the rapid exploration of chemical space.

By comparing computational data with the collated experimental outcomes and balancing accuracy with expense, it had been hoped to determine the cheapest computational methods that qualitatively reproduced the experimental data, i.e. whether ligand combinations would self-sort into homoleptic or heteroleptic species. This approach required a comparison between the calculated energies of these two extremes of the self-assembly outcomes; namely, complete narcissistic self-sorting, to give purely homoleptic species, and total integrative self-assembly, to give the targeted heteroleptic assemblies (Figure 1a).

As *cis*-$Pd_2\mathbf{L}_2\mathbf{L'}_2$ MOCs were being targeted specifically, the heteroleptic assemblies requiring computational investigation were straightforward to enumerate. *cis*- and *trans*-$[Pd_2(\mathbf{1})_2(\mathbf{2})_2]^{4+}$ cage models for all 12 heteroleptic ligand combinations were built[38] using *stk*[39] based on ligand conformers generated with the ETKDG algorithm[33] in RDKit.[34] These were initially optimised using UFF in the General Utility Lattice Program (GULP),[40] followed by semi-empirical GFN2-xTB[41] methods and subsequently by DFT (PBE0/Def2-SVP/D3BJ/PCM(DMSO)).[42] From these, single-point energies (SPEs) for the minimised structures were calculated. Importantly, if the xTB data could be shown to reliably replicate those of DFT methods, the significantly cheaper semi-empirical methods could be used for high-throughput screening.

The data was initially examined to support the conclusion that the two experimentally successful heteroleptic $[Pd_2\mathbf{1}^{\mathbf{DBF}}{}_2\mathbf{2}_2]^{4+}$ systems were indeed the *cis* isomers. Pleasingly, although unsurprisingly, both xTB and DFT data showed a clear preference for the *cis* isomers over the *trans* (Tables S3 and S4).

With SPEs for all 12 possible heteroleptic cages in-hand, the more challenging problem of predicting the lowest energy homoleptic assemblies subsequently required attention. For previously reported ligands, whose homoleptic assemblies have been identified, the complexity of this task is much reduced. Thus, the SPE values (GFN2-xTB) for the xTB-optimised structures of $[Pd_6(\mathbf{1}^{\mathbf{DBF}})_6]^{12+}$, $[Pd_{12}(\mathbf{1}^{\mathbf{Ph}})_{24}]^{24+}$ and $[Pd_{30}(\mathbf{1}^{\mathbf{Th}})_{30}]^{30+}$ were readily computed.

To expand the chemical space being explored, however, it was desirable to assume no *a priori* structural information, allowing analysis of ligands for which experimental self-assembly data are ambiguous or unknown. As a preliminary exploration, geometry-optimised structures and SPEs (GFN2-xTB) were calculated for $[Pd_n\mathbf{1}^{\mathbf{DBF}}{}_{2n}]^{2n+}$ assemblies of common Pd_nL_{2n} cage topologies (n = 2, 3, 4, 6, 12 and 24). Gratifyingly, the lowest energy structure from these was identified as the Pd_6L_{12} architecture that has previously been shown to form experimentally (Figure 7).[27] This approach also successfully

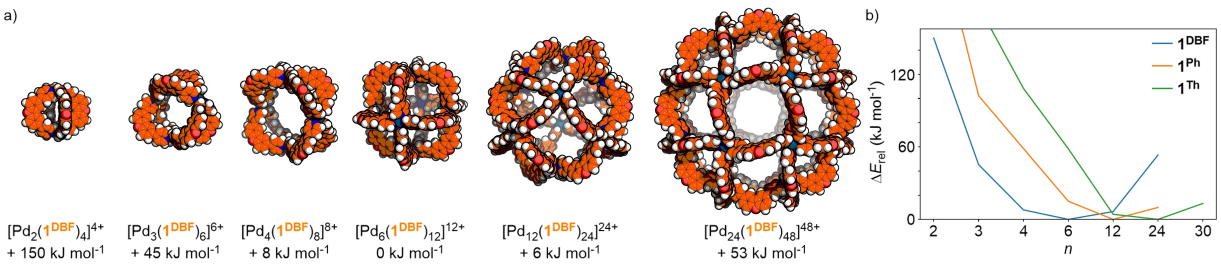

Figure 7. a) Geometry-optimised (GFN2-xTB) structures of $[Pd_n(\mathbf{1}^{\mathbf{DBF}})_{2n}]^{2n+}$ cages with their relative single point energies per Pd(II) ion, ΔE_{rel} (GFN2-xTB). b) ΔE_{rel} versus topology nuclearity, *n*, for ligands **1**.

predicted the experimentally observed $Pd_{12}L_{24}$ topology for $\mathbf{1}^{Ph}$, and $Pd_{24}L_{48}$ for $\mathbf{1}^{Th}$, although the purported thermodynamic $Pd_{30}L_{60}$ product for the latter appeared less stable (Figure 7b). It is noted that implicit solvent was required within the model to obtain results congruent with experimental data, highlighting the importance of identifying essential factors for useful computational modelling whilst omitting those that increase expense without notable benefit.

For the homoleptic assemblies of ligands **2**, initial computational exploration was limited to Pd_2L_4 structures as these species had been detected by various techniques (MS or SCXRD) for all four ligands, and the precise structure of possible Pd_3L_6 assemblies remained ambiguous. All four xTB-optimised structures and SPEs were calculated using the approach outlined above.

With a complete set of SPE values in-hand, hypothetical equilibria between homoleptic and heteroleptic species were examined:

$$[Pd_6(\mathbf{1}^{DBF})_{12}]^{12+} + 3[Pd_2(\mathbf{2})_4]^{4+} \rightleftharpoons 6[Pd_2(\mathbf{1}^{DBF})_2(\mathbf{2})_2]^{4+}$$

$$[Pd_{12}(\mathbf{1}^{Ph})_{24}]^{24+} + 6[Pd_2(\mathbf{2})_4]^{4+} \rightleftharpoons 12[Pd_2(\mathbf{1}^{Ph})_2(\mathbf{2})_2]^{4+}$$

$$[Pd_{30}(\mathbf{1}^{Th})_{60}]^{60+} + 15[Pd_2(\mathbf{2})_4]^{4+} \rightleftharpoons 30[Pd_2(\mathbf{1}^{Th})_2(\mathbf{2})_2]^{4+}$$

The sums of SPEs (Σ) were used to calculate the difference in energies ($\Delta E = \Sigma_{homo}$-Σ_{hetero}) between the homoleptic and heteroleptic systems, according to the balanced equations:

$$\Sigma_{homo} = [Pd_n(\mathbf{1})_{2n}]^{2n+} + \frac{n}{2}[Pd_2(\mathbf{2})_4]^{4+}$$

$$\Sigma_{hetero} = n[Pd_2(\mathbf{1})_2(\mathbf{2})_2]^{4+}$$

For comparing values, these were then divided by n to give the energy difference per mole of heteroleptic cage, $\Delta E_{het.}$ Positive values of ΔE_{het} would thus indicate the heteroleptic assembly was energetically favourable compared to the homoleptic species.

While the resultant energy balances (Table 1) broadly coincided with the experimental data, there were some noticeable discrepancies. *cis*-$[Pd_2(\mathbf{1}^{DBF})_2(\mathbf{2}^{DBF})_2]^{4+}$ and *cis*-$[Pd_2(\mathbf{1}^{Ph})_2(\mathbf{2}^{DBF})_2]^{4+}$ had the most positive ΔE_{het} values, suggesting the heteroleptic cages should be favoured, in contrast to the narcissistic self-sorting experimentally observed. The formation of *cis*-$[Pd_2(\mathbf{1}^{DBF})_2(\mathbf{2}^{Py})_2]^{4+}$ was ostensibly favoured, but to a small degree (2 kJ mol^{-1}), while a very small, negative ΔE_{het} value (−0.05 kJ mol^{-1}) was obtained for *cis*-$[Pd_2(\mathbf{1}^{DBF})_2(\mathbf{2}^{Ph})_2]^{4+}$; these values are within the margin of error of the method.

To investigate whether a higher level of theory for the geometry optimisations and SPE calculations would generate results more congruent with experiment, two heteroleptic systems were chosen for more expensive computational studies: *cis*-$[Pd_2(\mathbf{1}^{DBF})_2(\mathbf{2}^{Th})_2]^{4+}$ and *cis*-$[Pd_2(\mathbf{1}^{DBF})_2(\mathbf{2}^{Py})_2]^{4+}$. These were chosen as $\mathbf{2}^{Th}$ had unambiguously shown formation of a Pd_2L_4 homoleptic cage in solution, and the SCXRD structure of $Pd_2(\mathbf{2}^{Py})_4$ had been obtained, simplifying the homoleptic species to be modelled.

The xTB-optimised structures for the three homoleptic cages with $\mathbf{1}^{DBF}$, $\mathbf{2}^{Py}$ and $\mathbf{2}^{Th}$ were both re-optimised and their SPEs calculated at the DFT level of theory (PBE0/Def2-SVP/D3BJ/PCM(DMSO)). Disappointingly, these new computed data suggested the homoleptic systems would be favoured in both instances by more than 50 kJ mol^{-1} (Table 2 and Table S5), contrary to the experimental outcomes.

With the level of molecular complexity of MOCs there is no single 'gold-standard' against which calculations for these systems can be compared. Consequently, it seemed prudent to investigate different DFT methods (with both geometry optimisation and SPEs). PBE0, B3LYP, B97D3, and HSE methods were all used to probe the equilibrium between homoleptic and heteroleptic species with the assemblies of $\mathbf{1}^{DBF}$ and $\mathbf{2}^{Py}$.

PBE0, B3LYP and B97D3 showed qualitatively the same story – the homoleptic systems were favoured in all cases (Table 2). This remained true when using the SCXRD structure of $[Pd_2(\mathbf{2}^{Py})_4]^{4+}$ as the starting geometry for the DFT-optimised structure; indeed, this was universally ~20 kJ mol^{-1} more stable than the *stk*-generated structure.

HSE-level SPE calculations using PBE0-optimised structures as input suggested the heteroleptic cage should be favoured (ΔE_{het} = 12.1 kJ mol^{-1}), consistent with experimental results. Conversely, using HSE-optimised structures led to a negligible difference in the SPEs of the homo- and heteroleptic systems (ΔE_{het} = 0.4 kJ mol^{-1}). Once again, using the SCXRD of the homoleptic $[Pd_2(\mathbf{2}^{Py})_4]^{4+}$ as initial input before geometry

Table 1. ΔE_{het} values for $[Pd_n(\mathbf{1})_{2n}]^{n+} + \frac{n}{2}[Pd_2(\mathbf{2})_4]^{4+} \rightleftharpoons n[Pd_2(\mathbf{1})_2(\mathbf{2})_2]^{4+}$ equilibria from GFN2-xTB calculated SPEs and geometry-optimised structures.

	$\mathbf{1}^{DBF}$	$\mathbf{1}^{Ph}$	$\mathbf{1}^{Th}$
$\mathbf{2}^{DBF}$	26	3	−16
$\mathbf{2}^{Py}$	2.0	−15	−178
$\mathbf{2}^{Ph}$	−0.05	−28	−53
$\mathbf{2}^{Th}$	−6.7	−33	−54

Table 2. ΔE_{het} values for $[Pd_6(\mathbf{1}^{DBF})_{12}]^{12+} + 3[Pd_2(\mathbf{2}^{Py})_4]^{4+} \rightleftharpoons 6[Pd_2(\mathbf{1}^{DBF})_2(\mathbf{2}^{Py})_2]^{4+}$ equilibrium.

Computational method		ΔE_{het} (kJ mol^{-1})	
Geometry	SPE		
GFN2-xTB	GFN2-xTB	2.0	—[a]
GFN2-xTB	PBE0	−58.0	(−75.3)[b]
PBE0	PBE0	−58.0	(−75.3)[b]
PBE0	B3LYP	−68.5	(−88.0)[b]
B3LYP	B3LYP	−69.0	(−87.7)[b]
PBE0	B97D3	−68.6	(−86.2)[b]
B97D3	B97D3	−68.7	(−85.4)[b]
PBE0	HSE	12.1	(22.3)[b]
HSE	HSE	0.4	(−7.5)[b]

[a] Not calculated. [b] SCXRD structure used for geometry of $[Pd_2(\mathbf{2}^{Py})_4]^{4+}$.

optimisation caused the SPE calculations to indicate the homoleptic species were thermodynamically favoured ($\Delta E_{het} = -7.5$ kJ mol^{-1}), albeit by a small amount (Table 2).

With a view to establishing high-throughput computations, static models of the cages had been used. A downside of this approach is that it effectively ignores entropic contributions and is rather an analysis of the enthalpy of the systems. As such, when entropic considerations dominate the self-assembly process,[23e,43] this approach may not be appropriate. It became clear that fundamental components of the models necessary for qualitative reproduction of experimental results were being overlooked. It is anticipated that interactions with solvent and counterions, and conformational flexibility, also play significant roles. The precise manner of these, and their relative impact on individual systems, however, remains unknown. Without a clear indication of how such additional interactions might be reliably incorporated into the models at this stage, further studies were abandoned.

Conclusions

Attempting to derive a high-throughput computational workflow to expedite the discovery of *cis*-$Pd_2\mathbf{L}_2\mathbf{L'}_2$ heteroleptic MOCs, a combined experimental and computational study was undertaken. Based on the well-known geometric complementarity approach, two sets of ligands (with converging and diverging coordination vectors) were examined in a combinatorial fashion for integrative self-assembly with Pd(II). Computational modelling, in the form of relatively simple geometric analyses, as well as more expensive geometry-optimisations and single-point energy calculations, were performed to post-rationalise the experimental results.

Geometric analysis of ligand libraries was successful in rapidly identifying pairs of complementary ligands for integrative self-assembly, demonstrating the viability of this simple approach. For ligands **1**, with limited conformational freedom, relatively inexpensive xTB calculations were also able to mirror experimental results in identifying products of self-assembly. Extending this approach to more flexible ligands, however, presented significant challenges in predicting the topology of the thermodynamically most stable assemblies. The use of 'static' approximations of dynamic structures[44] and single-molecule models (i.e. without explicit anions/solvent) likely contributed to the lack of success in using computed energy balances to predict self-assembly outcomes.

The need to synthesise ligands and experimentally examine their self-assembly would obviously negate the purpose of computationally-informed design. Additionally, in instances where the topography of the thermodynamic landscape is more complex than can be approximated to an individual assembly (as with $\mathbf{2}^{Ph}$), or the precise nature of the structure(s) formed is ambiguous (as with $[Pd_3(\mathbf{2}^{Py})_6]^{6+}$), experimental data might be of limited use.

The overarching conclusion from this work is that many factors that are often omitted for the sake of computational simplicity may hold the key to successfully modelling the thermodynamics of self-assembly. Elucidating what these are and how they can be effectively incorporated into modelling studies will be paramount to useful *in silico* exploration of chemical space in the future.

Author Contributions

AT: Conceptualization, Writing – Original Draft Preparation, Data Curation, Software, Methodology, Investigation. **WS**: Writing – Review & Editing, Investigation. **VP**: Writing – Review & Editing, Data Curation, Methodology, Investigation. **CJTC**: Writing – Review & Editing, Investigation **LM**: Writing – Review & Editing, Investigation (SCXRD). **BDE**: Writing – Review & Editing, Investigation. **RLG**: Writing – Review & Editing, Investigation. **KEJ**: Conceptualization, Supervision, Funding Acquisition, Writing – Review & Editing. **JEML**: Conceptualization, Writing – Original Draft Preparation, Supervision, Funding Acquisition, Methodology, Investigation, Resources, Project Administration.

Supporting Information Summary

The authors have cited additional references within the Supporting Information.[45-76]

Acknowledgements

Dr Georgia Orton is thanked for assistance in the collection of SCXRD data. We acknowledge Diamond Light Source for time on Beamline I19 under Proposal CY28766. We are grateful to the Imperial College High Performance Computing Service (https://doi.org/10.14469/hpc/2232) for providing computational resources for this study. This work was funded by the European Union - Next Generation EU, Mission 4 Component 1 CUP E13 C22002930006. AT acknowledges the CINECA award under the ISCRA initiative for the availability of high-performance computing resources and support. RLG thanks the Royal Society for a University Research Fellowship (URF\R1\191432), and the EPSRC under EP/W01601X/1 for financial support. KEJ acknowledges the Royal Society for a University Research Fellowship and Enhancement Award and the ERC through Agreement No. 758370 (ERC-StG-PE5-CoMMaD). JEML thanks the Royal Society for a University Research Fellowship (URF\R1\221740 and RF\ERE\221016) and acknowledges support from the University of Birmingham.

Conflict of Interests

The authors declare no conflict of interest.

Data Availability Statement

The data that support the findings of this study, including structure files and properties, are available at https://doi.org/10.5281/zenodo.13923130 and in the supplementary material of this article.

Keywords: Coordination cage · Heteroleptic · Self-assembly · High-throughput · Computational screening

[1] a) D. Zhang, T. K. Ronson, J. R. Nitschke, *Acc. Chem. Res.* **2018**, *51*, 2423–2436; b) A. J. Gosselin, C. A. Rowland, E. D. Bloch, *Chem. Rev.* **2020**, *120*, 8987–9014; c) S. Lee, H. Jeong, D. Nam, M. S. Lah, W. Choe, *Chem. Soc. Rev.* **2021**, *50*, 528–555; d) J. E. M. Lewis, *Chem. Commun.* **2022**, *58*, 13873–13886; e) T. Tateishi, M. Yoshimura, S. Tokuda, F. Matsuda, D. Fujita, S. Furukawa, *Coord. Chem. Rev.* **2022**, *467*, 414612; f) A. J. McConnell, *Chem. Soc. Rev.* **2022**, *51*, 2957–2971; g) R. Banerjee, D. Chakraborty, P. S. Mukherjee, *J. Am. Chem. Soc.* **2023**, *145*, 7692–7711.

[2] a) C. J. Brown, F. D. Toste, R. G. Bergman, K. N. Raymond, *Chem. Rev.* **2015**, *115*, 3012–3035; b) C. Tan, D. Chu, X. Tang, Y. Liu, W. Xuan, Y. Cui, *Chem. Eur. J.* **2019**, *25*, 662–672; c) Y. Xue, X. Hang, J. Ding, B. Li, R. Zhu, H. Pang, Q. Xu, *Coord. Chem. Rev.* **2021**, *430*, 213656; d) R. Ham, C. J. Nielsen, S. Pullen, J. N. H. Reek, *Chem. Rev.* **2023**, *123*, 5225–5261; e) J. Wang, T. A. Young, F. Duarte, P. J. Lusby, *J. Am. Chem. Soc.* **2020**, *142*, 17743–17750; f) M. D. Ludden, C. G. P. Taylor, M. B. Tipping, J. S. Train, N. H. Williams, J. C. Dorrat, K. L. Tuck, M. D. Ward, *Chem. Sci.* **2021**, *12*, 14781–14791; g) A. C. Ghosh, A. Legrand, R. Rajapaksha, G. A. Craig, C. Sassoye, G. Balázs, D. Farrusseng, S. Furukawa, J. Canivet, F. M. Wissner, *J. Am. Chem. Soc.* **2022**, *144*, 3626–3636; h) D. O. Bobylev, J. Ruijter, D. A. Poole III, S. Matthew, B. de Bruin, J. N. H. Reek, *Angew. Chem. Int. Ed.* **2023**, *62*, e202218162; i) Y. Yang, X. Jing, Y. Shi, Y. Wu, C. Duan, *J. Am. Chem. Soc.* **2023**, *145*, 10136–10148.

[3] a) A. Galan, P. Ballester, *Chem. Soc. Rev.* **2016**, *45*, 1720–1737; b) P. Mal, B. Breiner, K. Rissanen, J. R. Nitschke, *Science* **2009**, *324*, 1697–1699; c) M. Yamashina, Y. Sei, M. Akita, M. Yoshizawa, *Nat. Commun.* **2014**, *5*, 4662; d) M. Canton, A. B. Grommet, L. Pesce, J. Gemen, S. Li, Y. Diskin-Posner, A. Credi, G. M. Pavan, K. Andréasson, R. Klajn, *J. Am. Chem. Soc.* **2020**, *142*, 14557–14565; e) S. Hasegawa, S. L. Meichsner, J. J. Holstein, A. Baksi, M. Kasanmascheff, G. H. Clever, *J. Am. Chem. Soc.* **2021**, *143*, 9718–9723; f) J. C. Dorrat, R. J. Young, C. G. P. Taylor, M. B. Tipping, A. J. Blok, D. R. Turner, A. I. McKay, S. Ovenden, M. D. Ward, G. H. Dennison, K. L. Tuck, *Dalton Trans.* **2023**, *52*, 11802–11814.

[4] a) D. Zhang, T. K. Ronson, Y.-Q. Zou, J. R. Nitschke, *Nat. Rev. Chem.* **2021**, *5*, 168–182; b) A. Ghosh, J. Pruchyathamkorn, C. F. Espinosa, J. R. Nitschke, *J. Am. Chem. Soc.* **2024**, *146*, 2568–2573; c) L.-J. Wang, S. Bai, Y.-F. Han, *J. Am. Chem. Soc.* **2022**, *144*, 16191–16198; d) R. Tabuchi, H. Takezawa, M. Fujita, *Angew. Chem. Int. Ed.* **2022**, *61*, e202208866; e) D. Prajapati, P. Bhandari, E. Zangrando, P. S. Mukherjee, *Chem. Sci.* **2024**, *15*, 3616–3624.

[5] a) R. Custelcean, *Chem. Soc. Rev.* **2014**, *43*, 1813–1824; b) G. H. Clever, P. Punt, *Acc. Chem. Res.* **2017**, *50*, 2233–2243; c) D. Preston, K. M. Patil, A. T. O'Neil, R. A. S. Vasdev, J. A. Kitchen, P. E. Kruger, *Inorg. Chem. Front.* **2020**, *7*, 2990–3001; d) B. J. J. Timmer, T. J. Mooibroek, *Chem. Commun.* **2021**, *57*, 7184–7187; e) A. P. Birvé, H. D. Patel, J. R. Price, W. M. Bloch, T. Fallon, *Angew. Chem. Int. Ed.* **2022**, *61*, e202115468; f) V. Sivalingam, S. Krishnaswamy, D. K. Chand, *Chem. Eur. J.* **2023**, *29*, e202300891; g) S. Sudan, D. W. Chen, C. Berton, F. Fadaei-Tirani, K. Severin, *Angew. Chem. Int. Ed.* **2023**, *62*, e202218072; h) W.-L. Jiang, B. Huang, X.-L. Zhao, X. Shi, H.-B. Yang, *Chem* **2023**, *9*, 26555–2668.

[6] a) E. G. Percástegui, *Chem. Commun.* **2022**, *58*, 5055–5071; b) S. Ganta, D. K. Chand, *Inorg. Chem.* **2018**, *57*, 3634–3645; c) A. Platzek, S. Juber, C. Yurtseven, S. Hasegawa, L. Schneider, C. Drechsler, K. E. Ebbert, R. Rudolf, Q.-Q. Yan, J. J. Holstein, L. V. Schäfer, G. H. Clever, *Angew. Chem. Int. Ed.* **2022**, *61*, e202209305; d) T. K. Ronson, J. P. Carpenter, J. R. Nitschke, *Chem* **2022**, *8*, 557–568.

[7] a) S. Pullen, J. Tessarolo, G. H. Clever, *Chem. Sci.* **2021**, *12*, 7269–7293; b) J. E. M. Lewis, *Trends Chem.* **2023**, *5*, 717–719.

[8] C. T. McTernan, J. A. Davies, J. R. Nitschke, *Chem. Rev.* **2022**, *122*, 10393–10437.

[9] a) M. Han, D. M. Engelhard, G. H. Clever, *Chem. Soc. Rev.* **2014**, *43*, 1848–1860; b) S. Saha, I. Regeni, G. H. Clever, *Coord. Chem. Rev.* **2018**, *374*, 1–14; c) A. Schmidt, A. Casini, F. E. Kühn, *Coord. Chem. Rev.* **2014**, *275*, 19–36; d) Z. T. Avery, J. L. Algar, D. Preston, *Trends Chem.* **2024**, *6*, 352–364.

[10] D. A. McMorran, P. J. Steel, *Angew. Chem. Int. Ed.* **1998**, *37*, 3295–3297.

[11] a) J. E. M. Lewis, J. D. Crowley, *ChemPlusChem* **2020**, *85*, 815–827; b) D. Tripathy, N. B. Debata, K. C. Naik, H. S. Sahoo, *Coord. Chem. Rev.* **2022**, *456*, 214396; c) D. Ogata, J. Yuasa, *Angew. Chem. Int. Ed.* **2019**, *58*, 18424–18428; d) J. E. M. Lewis, A. Tarzia, A. J. P. White, K. E. Jelfs, *Chem. Sci.* **2020**, *11*, 677–683; e) R.-J. Li, A. Marcus, F. Fadaei-Tirani, K. Severin, *Chem. Commun.* **2021**, *58*, 10023–10026; f) J. E. M. Lewis, *Angew. Chem. Int. Ed.* **2022**, *61*, e202212392; g) R.-J. Li, A. Tarzia, V. Posligua, K. E. Jelfs, N. Sanchez, A. Marcus, A. Baksi, G. H. Clever, F. Fadaei-Tirani, K. Severin, *Chem. Sci.* **2022**, *13*, 11912–11917; h) R. A. S. Vasdev, D. Preston, C. A. Casey-Stevens, V. Martí-Centelles, P. J. Lusby, A. L. Garden, J. D. Crowley, *Inorg. Chem.* **2023**, *62*, 1833–1844; i) P. Molinska, A. Tarzia, L. Male, K. E. Jelfs, J. E. M. Lewis, *Angew. Chem. Int. Ed.* **2023**, *62*, e202315451; j) B. E. Barber, E. M. G. Jamieson, L. E. M. White, C. T. McTernan, *Chem* **2024**, *10*, 2792–2806; k) R. G. Siddique, J. C. McMurtrie, J. K. Clegg, *Dalton Trans.* **2024**, *53*, 11237–11241; l) M. Parbin, V. Sivalingam, D. K. Chand, *Angew. Chem. Int. Ed.* **2024**, *63*, e202410219.

[12] a) F. Li, L. F. Lindoy, *Aus. J. Chem.* **2019**, *72*, 731–741; b) M. Hardy, A. Lützen, *Chem. Eur. J.* **2020**, *26*, 13332–13346; c) L. K. Moree, L. A. V. Faulkner, J. D. Crowley, *Chem. Soc. Rev.* **2024**, *53*, 25–46; d) S. M. Jansze, M. D. Wise, A. V. Vologzhanina, R. Scopelliti, K. Severin, *Chem. Sci.* **2017**, *8*, 1901–1908; e) C. Shen, A. D. W. Kennedy, W. A. Donald, A. M. Torres, W. S. Price, J. E. Beves, *Inorg. Chim. Acta.* **2017**, *458*, 122–128; f) D. Preston, J. J. Sutton, K. C. Gordon, J. D. Crowley, *Angew. Chem. Int. Ed.* **2018**, *57*, 8659–8663; g) L. S. Lisboa, J. A. Findlay, L. J. Wright, C. G. Hartinger, J. D. Crowley, *Angew. Chem. Int. Ed.* **2020**, *59*, 11101–11107; h) L. S. Lisboa, D. Preston, C. J. McAdam, L. J. Wright, C. G. Hartinger, J. D. Crowley, *Angew. Chem. Int. Ed.* **2022**, *61*, e202201700; i) A. C. Pearcy, L. S. Lisboa, D. Preston, N. B. Page, T. Lawrence, L. J. Wright, C. Hartinger, J. D. Crowley, *Chem. Sci.* **2023**, *14*, 8615–8623.

[13] a) W. M. Bloch, G. H. Clever, *Chem. Commun.* **2017**, *53*, 8506–8516; b) S. Pullen, G. H. Clever, *Acc. Chem. Res.* **2018**, *51*, 3052–3064; c) D. Bardhan, D. K. Chand, *Chem. Eur. J.* **2019**, *25*, 12241–12269; d) C.-B. Tian, Q.-F. Sun, *Chem. Eur. J.* **2023**, *29*, e202300195.

[14] a) A. M. Johnson, O. Moshe, A. S. Gamboa, B. W. Langloss, J. F. K. Limtiaco, C. K. Larive, R. J. Hooley, *Inorg. Chem.* **2011**, *50*, 9430–9442; b) A. M. Johnson, R. J. Hooley, *Inorg. Chem.* **2011**, *50*, 4671–4673; c) J. Tessarolo, E. Benchimol, A. Jouaiti, M. W. Hosseini, G. H. Clever, *Chem. Commun.* **2023**, *59*, 3467–33470; d) R. G. DiNardi, S. Rasheed, S. S. Capomolla, M. H. Chak, I. A. Middleton, L. K. Macreadie, J. P. Violi, W. A. Donald, P. J. Lusby, J. E. Beves, *J. Am. Chem. Soc.* **2024**, *146*, 21196–21202.

[15] M. Yoshizawa, M. Nagao, K. Kumazawa, M. Fujita, *J. Organomet. Chem.* **2005**, *690*, 5383–5388.

[16] a) R. Zhu, W. M. Bloch, J. J. Holstein, S. Mandal, L. V. Schäfer, G. H. Clever, *Chem. Eur. J.* **2018**, *24*, 12976–12982; b) R.-J. Li, J. Tessarolo, H. Lee, G. H. Clever, *J. Am. Chem. Soc.* **2021**, *143*, 3865–3873; c) B. Chen, J. J. Holstein, A. Platzek, L. Schneider, K. Wu, G. H. Clever, *Chem. Sci.* **2022**, *13*, 1829–1834.

[17] D. Preston, J. E. Barnsley, K. C. Gordon, J. D. Crowley, *J. Am. Chem. Soc.* **2016**, *138*, 10578–10585.

[18] a) S. Samantray, S. Krishnaswamy, D. K. Chand, *Nat. Commun.* **2020**, *11*, 880; b) D. Preston, J. D. Evans, *Angew. Chem. Int. Ed.* **2023**, *62*, e2202314378.

[19] a) W. M. Bloch, Y. Abe, J. J. Holstein, C. M. Wandtke, B. Dittrich, G. H. Clever, *J. Am. Chem. Soc.* **2016**, *138*, 13750–13755; b) W. M. Bloch, J. J. Holstein, W. Hiller, G. H. Clever, *Angew. Chem. Int. Ed.* **2017**, *56*, 8285–8289; c) S. Saha, B. Holzapfel, Y.-T. Chen, K. Terlinden, P. Lill, C. Gatsogiannis, H. Rehage, G. H. Clever, *J. Am. Chem. Soc.* **2018**, *140*, 17384–17388; d) K. Wu, J. Tessarolo, A. Baksi, G. H. Clever, *Angew. Chem. Int. Ed.* **2022**, *61*, e202205725; e) E. Benchimol, I. Regeni, B. Zhang, M. Kabiri, J. J. Holstein, G. H. Clever, *J. Am. Chem. Soc.* **2024**, *146*, 6905–6911.

[20] a) S. Sudan, J.-J. Li, S. M. Jansze, A. Platzek, R. Rudolf, G. H. Clever, F. Fadaei-Tirani, R. Scopelliti, K. Severin, *J. Am. Chem. Soc.* **2021**, *143*, 1773–1778; b) R.-J. Li, F. Fadaei-Tirani, R. Scopelliti, K. Severin, *Chem. Eur. J.* **2021**, *27*, 9439–9445; c) K. Wu, B. Zhang, C. Drechsler, J. J. Holstein, G. H. Clever, *Angew. Chem. Int. Ed.* **2021**, *60*, 6403–6407; d) J. Tessarolo, H. Lee, E. Sakuda, K. Umakoshi, G. H. Clever, *J. Am. Chem. Soc.* **2021**, *143*, 6339–6344; e) K. E. Ebbert, E. Benchimol, A. Platzek, C. Dreschsler, J. Openy, S. Hasegawa, J. J. Holstein, G. H. Clever, *Angew. Chem. Int. Ed.* **2024**, *63*, e202413323.

[21] a) R.-J. Li, J. de Montmolling, F. Fadaei-Tirani, R. Scopelliti, K. Severin, *Dalton Trans.* **2023**, *52*, 6451–6456; b) Y. Liu, S.-H. Liao, W.-T. Dai, Q. Bai, S. Lu, H. Wang, X. Li, Z. Zhang, P. Wang, W. Lu, Q. Zhang, *Angew. Chem. Int. Ed.* **2023**, *62*, e202217215.

[22] a) T. Abe, N. Sanada, K. Tekeuchi, A. Okazawa, S. Hiraoka, *J. Am. Chem. Soc.* **2023**, *145*, 28061–28074; b) K. Wu, E. Benchimol, A. Baksi, G. H. Clever, *Nat. Chem.* **2024**, *16*, 584–591.

[23] a) T. K. Piskorz, V. Martí-Centelles, T. A. Young, P. J. Lusby, F. Duarte, *ACS Catal.* **2022**, *12*, 5806–5826; b) A. Tarzia, K. E. Jelfs, *Chem. Commun.* **2022**, *58*, 3717–3730; c) S. Hiraoka, S. Takahashi, H. Sato, *Chem. Rev.* **2021**, *21*, 443–459; d) A. Tarzia, E. H. Wolpert, K. E. Jelfs, G. M. Pavan, *Chem. Sci.* **2023**, *14*, 12506–12517; e) D. A. Poole III, E. O. Bobylev, S. Mathew, J. N. H. Reek, *Chem. Sci.* **2022**, *13*, 10141–10148; f) E. O. Bobylev, D. A. Poole III, B. de Bruin, J. N. H. Reek, *Chem. Sci.* **2021**, *12*, 7696–7705; g) T. A. Young, R. Gheorghe, F. Duarte, *J. Chem. Inf. Model.* **2020**, *60*, 3546–3557; h) A. Kondinski, A. Menon, D. Nurkowski, F. Farazi, S. Mosbach, J. Akroyd, M. Kraft, *J. Am. Chem. Soc.* **2022**, *144*, 11713–11728; i) T. Abe, K. Takeuchi, M. Higashi, H. Sato, S. Hiraoka, *Nat. Commun.* **2024**, *15*, 7630.

[24] a) T. K. Piskorz, V. Martí-Centelles, R. L. Spicer, F. Duarte, P. J. Lusby, *Chem. Sci.* **2023**, *14*, 11300–11331; b) T. A. Young, V. Martí-Centelles, J. Wang, P. J. Lusby, F. Duarte, *J. Am. Chem. Soc.* **2020**, *142*, 1300–1310.

[25] D. A. Poole III, E. O. Bobylev, S. Matthew, J. N. H. Reek, *Chem. Sci.* **2020**, *11*, 12350–12357.

[26] A. Tarzia, J. E. M. Lewis, K. E. Jelfs, *Angew. Chem. Int. Ed.* **2021**, *60*, 20879–20887.

[27] E. O. Bobylev, B. de Bruin, J. N. H. Reek, *Inorg. Chem.* **2021**, *60*, 12498–12505.

[28] M. Tominaga, K. Suzuki, M. Kawano, T. Kusukawa, T. Ozeki, S. Sakamoo, K. Yamaguchi, M. Fujita, *Angew. Chem. Int. Ed.* **2004**, *43*, 5621–5625.

[29] D. Fujita, Y. Ueda, S. Sato, H. Yokoyama, N. Mizuno, T. Kumasaka, M. Fujita, *Chem* **2016**, *1*, 91–101.

[30] Q.-F. Sun, J. Iawsa, D. Ogawa, Y. Ishido, S. Sato, T. Ozeki, Y. Sei, K. Yamaguchi, M. Fujita, *Science* **2010**, *328*, 1144–1147.

[31] a) H. S. Sahoo, D. K. Chand, *Dalton Trans.* **2010**, *39*, 7223–7225; b) J. D. Crowley, E. L. Gavey, *Dalton Trans.* **2010**, *39*, 4035–4037; c) L.-P. Zhou, Q.-F. Sun, *Chem. Commun.* **2015**, *51*, 16767–16770; d) Q. Lin, B. Kauffmann, J. Zhang, C. Ma, D. Luo, Q. Gan, *Chem. Commun.* **2018**, *54*, 13447–13450; e) P. J. Steel, D. A. McMorran, *Chem. Asian J.* **2019**, *14*, 1098–1101; f) W. M. Bloch, S. Horiuchi, J. J. Holstein, C. Drechsler, A. Wuttke, W. Hiller, R. A. Mata, G. H. Clever, *Chem. Sci.* **2023**, *14*, 1524–1531.

[32] D. M. Engelhard, S. Freye, K. Grohe, M. John, G. H. Clever, *Angew. Chem. Int. Ed.* **2012**, *51*, 4747–4750.

[33] S. Wang, J. Witek, G. A. Landrum, S. Riniker, *J. Chem. Inf. Model.* **2020**, *60*, 2044–2058.

[34] RDKit: Open-source cheminformatics. https://www.rdkit.org (accessed March 04, 2022).

[35] A. K. Rappe, C. J. Casewit, K. S. Colwell, W. A. Goddard III, W. M. Skiff, *J. Am. Chem. Soc.* **1992**, *114*, 10024–10035.

[36] Each of these ligand conformer libraries was filtered after UFF optimisation with heavy-atom root mean square deviation (RMSD) and relative UFF strain energy thresholds of 0.2 Å and 5 kJ mol^{-1}, respectively, applied. These were further pruned to exclude those with a torsion between binding sites (Figure S163) larger than 10°, as formation of *cis*-$Pd_2\mathbf{L}_2\mathbf{L'}_2$ heteroleptic architectures, within which ligand binding sites should be aligned, were being specifically targeted.

[37] https://github.com/andrewtarzia/simple het construction (accessed September 03, 2024).

[38] The supramolecular toolkit, https://github.com/lukasturcani/stk (accessed June 17, 2022).

[39] L. Turcani, A. Tarzia, F. T. Szczypiński, K. E. Jelfs, *J. Chem. Phys.* **2021**, *154*, 214102.

[40] a) J. D. Gale, *J. Chem. Soc., Faraday Trans.* **1997**, *93*, 629–637; b) J. D. Gale, A. L. Rohl, *Mol. Simul.* **2003**, *29*, 291–341.

[41] a) C. Bannwarth, S. Ehlert, S. Grimme, *J. Chem. Theory Comput.* **2019**, *15*, 1652–1671; b) M. Bursch, H. Neugebauer, S. Grimme, *Angew. Chem. Int. Ed.* **2019**, *58*, 11078–11087.

[42] a) C. Adamo, V. Barone, *J. Chem. Phys.* **1999**, *110*, 6158–6170; b) F. Weigend, R. Ahlrichs, *Phys. Chem. Chem. Phys.* **2005**, *7*, 3297–3305; c) S. Grimme, S. Ehrlich, L. Goerigk, *J. Comp. Chem.* **2011**, *32*, 1456–1465.

[43] F. J. Rizzuto, J. P. Carpenter, J. R. Nitschke, *J. Am. Chem. Soc.* **2019**, *141*, 9087–9095.

[44] A. E. Martín Díaz, J. E. M. Lewis, *Front. Chem.* **2021**, *9*, 706462.

[45] J. P. Byrne, J. A. Kitchen, O. Kotova, V. Leigh, A. P. Bell, J. J. Boland, M. Albrecht, T. Gunnlaugsson, *Dalton Trans.* **2014**, *43*, 196–209.

[46] S. Lee, Y. Hua, H. Park, A. H. Flood, *Org. Lett.* **2010**, *12*, 2100–2102.

[47] L. Zeng, Y. Xiao, J. Jiang, H. Fang, Z. Ke, L. Chen, J. Zhang, *Inorg. Chem.* **2019**, *58*, 10019–10027.

[48] M. Kato, H. Sano, T. Kiyobayashi, M. Yao, *ChemSusChem* **2020**, *13*, 2379–2385.

[49] C. R. Groom, I. J. Bruno, M. P. Lightfood, S. C. Ward, *Acta Cryst.* **2016**, *B72*, 171–179.

[50] Calculate Root-mean-square deviation (RMSD) of Two Molecules Using Rotation, GitHub, http://github.com/charnley/rmsd, version 1.5.1.

[51] E. O. Bobylev, D. A. Poole III, B. de Bruin, J. N. H. Reek, *Chem. Eur. J.* **2021**, *27*, 12667–12674.

[52] S. Ehlert, M. Stahn, S. Spicher, S. Grimme, *J. Chem. Theory Comput.* **2021**, *17*, 4250–4261.

[53] a) D. E. Coupry, M. A. Addicoat, T. Heine, *J. Chem. Theory Comput.* **2016**, *12*, 5215–5225; b) M. A. Addicoat, N. Vankova, I. F. Akter, T. Heine, *J. Chem. Theory Comput.* **2014**, *10*, 880–891.

[54] M. J. Frisch, G. W. Trucks, H. B. Schlegel, G. E. Scuseria, M. A. Robb, J. R. Cheeseman, G. Scalmani, V. Barone, G. A. Petersson, H. Nakatsuji, X. Li, M. Caricato, A. V. Marenich, J. Bloino, B. G. Janesko, R. Gomperts, B. Mennucci, H. P. Hratchian, J. V. Ortiz, A. F. Izmaylov, J. L. Sonnenberg, D. Williams-Young, F. Ding, F. Lipparini, F. Egidi, J. Goings, B. Peng, A. Petrone, T. Henderson, D. Ranasinghe, V. G. Zakrzewski, J. Gao, N. Rega, G. Zheng, W. Liang, M. Hada, M. Ehara, K. Toyota, R. Fukuda, J. Hasegawa, M. Ishida, T. Nakajima, Y. Honda, O. Kitao, H. Nakai, T. Vreven, K. Throssell, J. A. Montgomery, Jr., J. E. Peralta, F. Ogliaro, M. J. Bearpark, J. J. Heyd, E. N. Brothers, K. N. Kudin, V. N. Staroverov, T. A. Keith, R. Kobayashi, J. Normand, K. Raghavachari, A. P. Rendell, J. C. Burant, S. S. Iyengar, J. Tomasi, M. Cossi, J. M. Millam, M. Klene, C. Adamo, R. Cammi, J. W. Ochterski, R. L. Martin, K. Morokuma, O. Farkas, J. B. Foresman, D. J. Fox, *Gaussian 16, Revision C.01*, Gaussian, Inc., Wallingford CT **2016**.

[55] S. Grimme, *J. Comp. Chem.* **2006**, *27*, 1787–1799.

[56] A. D. Becke, *J. Chem. Phys.* **1993**, *98*, 5648–5652.

[57] C. Lee, W. Yang, R. G. Parr, *Phys. Rev. B* **1988**, *37*, 785–789.

[58] S. H. Vosko, L. Wilk, M. Nusair, *Can. J. Phys.* **1980**, *58*, 1200–1211.

[59] P. J. Stephens, F. J. Devlin, C. F. Chabalowski, M. J. Frisch, *J. Phys. Chem.* **1994**, *98*, 11623–11627.

[60] J. Heyd, E. G. Scuseria, M. Ernzerhof, *J. Chem. Phys.* **2003**, *118*, 8207–8215.

[61] J. Heyd, E. G. Scuseria, M. Ernzerhof, *J. Chem. Phys.* **2003**, *124*, 219906.

[62] A. D. Becke, E. R. Johnson, *J. Chem. Phys.* **2005**, *123*, 154101.

[63] E. R. Johnson, A. D. Becke, *J. Chem. Phys.* **2005**, *123*, 024101.

[64] E. R. Johnson, A. D. Becke, *J. Chem. Phys.* **2006**, *124*, 174104.

[65] H. Hirao, *J. Phys. Chem. A* **2011**, *115*, 9308–9313.

[66] H. Chang, W. Zheng, Y. Zheng, D. Zhu, J. Wang, *Tetrahedron Lett.* **2019**, *60*, 310–3211.

[67] L. M. Debefve, C. J. Pollock, *Phys. Chem. Chem. Phys.* **2021**, *23*, 24780–24788.

[68] N. Hoyas Pérez, P. S. Sherin, V. Posligua, J. L. Greenfield, M. J. Fuchter, K. E. Jelfs, M. K. Kuimova, J. E. M. Lewis, *Chem. Sci.* **2022**, *13*, 11368–11375.

[69] B. G. Janesko, T. M. Henderson, G. E. Scuseria, *Phys. Chem. Chem. Phys.* **2009**, *11*, 443–454.

[70] T. M. Henderson, A. F. Izmaylov, G. Scalmani, G. E. Scuseria, *J. Chem. Phys.* **2009**, *131*, 044108.

[71] A. Stroppa, G. Kresse, *New J. Phys.* **2008**, *10*, 063020.

[72] M. Holz, X. Mao, D. Seiferling, *J. Chem. Phys.* **1996**, *104*, 669–679.

[73] D. R. Allan, H. Nowell, S. A. Barnett, M. R. Warren, A. Wilcox, J. Christensen, L. K. Saunders, A. Peach, M. T. Hooper, L. Zaja, S. Patel, L. Cahill, R. Marshall, S. Trimnell, A. J. Foster, T. Bates, S. Lay, M. A. Williams, P. V. Hathaway, G. Winter, M. Gerstel, R. W. Wooley, *Crystals* **2017**, *7*, 336.

[74] O. V. Dolomanov, L. J. Bourhis, R. J. Gildea, J. A. K. Howard, H. Puschmann, *J. Appl. Crystallogr.* **2009**, *42*, 339–341.

[75] G. M. Sheldrick, *Acta Cryst.* **2015**, *A71*, 3–8.

[76] G. M. Sheldrick, *Acta Cryst.* **2015**, *C71*, 3–8.

Manuscript received: September 5, 2024
Accepted manuscript online: October 27, 2024
Version of record online: November 16, 2024

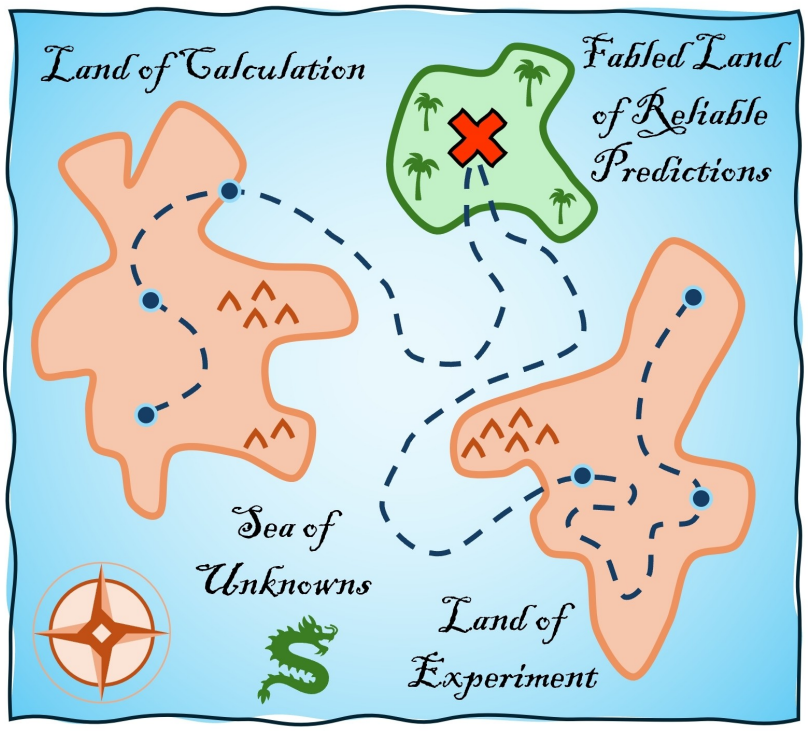

Dr. A. Tarzia, W. Shan, Dr. V. Posligua, C. J. T. Cox, Dr. L. Male, Dr. B. D. Egleston, Dr. R. L. Greenaway, Prof. Dr. K. E. Jelfs, Dr. J. E. M. Lewis**

1 – 10

A Combined Experimental and Computational Exploration of Heteroleptic *cis*-$Pd_2L_2L'_2$ Coordination Cages through Geometric Complementarity

Calculations based on ligand geometries and computed energies of coordination assemblies were compared against experimental results working towards rationalising the self-assembly of heteroleptic $Pd_2\mathbf{L}_2\mathbf{L}'_2$-type coordination cages. Valuable insights into the use and limitations of the approaches examined were gained in the continued development of high-throughput methods to aid molecular design.